17th World Conference on Earthquake Engineering, 17WCEE
Sendai, Japan - September 13th to 18th 2020

SEISMIC VULNERABILITY ANALYSIS OF ±800KV ULTRA-HIGH VOLTAGE DIRECT CURRENT（UHVDC）WALL BUSHING

H. Liang(1), Q. Xie(2)

(1) PHD Candidate, Department of Structural Engineering, Tongji University, 1710741@tongji.edu.cn
(2) PHD, Professor, Department of Structural Engineering, Tongji University, qxie@tongji.edu.cn

Abstract

In order to evaluate the seismic performance of a ±800kV UHVDC wall bushing, a finite element model of UHVDC wall bushing-valve hall system was established. Dynamic characteristics and time history analyses were carried out. The seismic vulnerability curves of the wall bushing with different levels of damage have been obtained based on strength and deformation aspects using the truncated incremental dynamic analysis (TIDA) method. The results show that the valve hall structure will almost double the seismic loading to the wall bushing. Stress responses at the base cross section of the wall bushing and the relative deformation responses at the end section of the insulating capacitor body are the vulnerable points under earthquakes. According to the proposed criteria for damage identification, the base cross section of outdoor bushing has the highest seismic vulnerability and would be very likely to experience severe damage under the earthquake with the fortification intensity (0.4 g). Furthermore, attentions have been risen to the potential electrical function problem caused by large relative deformation inside wall bushing. Therefore, the amplification of the valve hall structure cannot be neglected when evaluating the seismic performance of the wall bushing. Besides, it is urgent to take measures to decrease the stress responses at the base cross section of the wall bushing to improve its aseismic performance. What's more, it is also necessary to evaluate that to what extent will the relative deformation inside affect the electromagnetic stability of wall bushing and further give an explicit prescribed limit.

Keywords: Wall bushing; valve hall; amplification effect; truncated incremental dynamic analysis; vulnerability curve

1. Introduction

Substations and converter stations are indispensable part in power system and vulnerable to earthquakes [1]. The failure of any substation or converter may lead to power interruption and adversely affect disaster relief and rebuilding. Past earthquakes destroyed many substations and electric facilities. In 1994, during the Northridge Earthquake (in and around Los Angeles, CA, USA), the electric facilities in substations were broke down and the power supply was interrupted [2]. The 2008 Wenchuan Earthquake in China destroyed many insulators and bushings, which were always fractured at their base cross sections [3]. Additionally, the 2011 Tohoku Region Pacific Offshore Earthquake erupted with a magnitude of Mw 9.0, fracturing a total of 621 electric insulators, including many high voltage bushings [4]. The seismic performance of electric equipment is directly related to the normal functioning of power system. In recent years, in response to west-to-east gas and electricity transmission projects, ultra-high voltage direct current facilities began to be put into use in China southwest region [5-6]. Wall bushing, as a long cantilever beam with the feature of heavy weight and conspicuous flexibleness, plays an important role in connecting the converter valve in valve hall with other facilities in direct current field outside (Fig.1). Consequently, its seismic performance needs to be highly concerned and particularly researched to ensure the reliable operation and continuous electricity supply of the converter station.

Many scholars have conducted seismic research on bushing-type electric equipment, including the study on the dynamic characteristics and seismic responses of UHV bushing [7-8]; probe in the impact of dynamic characteristics of supports on seismic responses of bushing [9-10]; exploration on the mechanism of interaction between bushing and support structure [11-13]. It is numerically and experimentally verified that UHV bushings and insulators mounted on supporting structures (e.g., power transformers and steel frames) suffer amplified seismic loads compared with the ground motion due to the structural dynamics of the transformer tanks and steel frames. According to the Chinese Standards GB50260 [14] and the American Standards IEEE 693 [15], to evaluate the seismic performance of electric equipment, the equipment should be tested by mounted on a rigid adapter and the amplification factor of the support should be considered in the input of the test. And the amplification factors of 2.0 and 1.2 are specified specifically in Standards [14,15] for the bushings mounted on the transformer tanks (Fig.2(a)) and insulators installed on the steel frames (Fig.2(b)), respectively. However, the studies on seismic vulnerability of wall bushing are extremely rare nowadays and the regulation of amplification for wall bushing mounted on the gable wall of valve hall (Fig.1) is still vacant, which makes the corresponding research high necessity.

Fig. 1 - ±800kV UHVDC wall bushing-valve hall system

(a) bushings mounted on transformer tank (b) insulators mounted on steel frames

Fig. 2 - Bushings and insulators mounted on supporting structures

One of the common methods for assessing seismic vulnerability of electric equipment is using fragility curves [16-19], which predict the probability of a specified level of damage to the equipment based on ground motion parameters at the site of the equipment. The vulnerability analysis of critical electric facilities has following advantages: prediction of pre-earthquake disasters as an effective way of seismic risk assessment; improve the seismic resistance of the vulnerable equipment; provide a basis for estimating post-earthquake losses. Foreign researchers have developed seismic vulnerability curves of some bushing-type electrical equipment [20-23], and it is believed that the failure is caused by cracking at the root section of bushing due to insufficient material strength under the action of earthquake. It should be noted that some of previous studies made many simplifications while modeling and analyzing these bushing-type facilities such as in connection and inner structure of the bushing. There is gas or oil inside the wall bushing, hence, existence of even fine cracks will annihilate its insulation capability and then its performance will be affected. Besides, it has long been skeptical that the relative deformation inside the wall bushing will influence its insulation performance and electrical function. Considering the important role of wall bushings in a UHVDC convertor, it is necessary to evaluate their seismic vulnerability more reliably.

The primary objective of this research is to evaluate the seismic performance of a ±800kV UHVDC wall bushing in terms of vulnerability curves. A finite element model (FEM) of the wall bushing-valve hall system was established in Abaqus software. Based on TIDA method [26], vulnerability analysis was then conducted and corresponding vulnerability curves were obtained from strength aspect and for the first time from deformation aspect inside to rise attention to the potential electrical function problem caused by large relative deformation inside the wall bushing. The vulnerability curves are expected to further provide reference for improving the seismic performance of power facilities and provide data support for the seismic risk assessment of the power grid.

2 UHVDC wall bushing-valve hall system

2.1 Valve hall structure

Valve hall is an important building in converter station, which has excellent electromagnetic shielding functions. The length, width and height of the ±800 kV UHV valve hall are 82.7 m, 31.6 m and 29.2 m, respectively (Fig.3). The Z1 and Z2 columns are wide-flange-H-shaped member, with dimensions of 900×600×20×28 mm and 750×550×18×25 mm, respectively. The beams between the columns are square tubes, with cross sections of 250×250×10 mm. Additionally, braces in wide flange H shape are placed between the columns and beams, with dimensions of 250×250×12×12 mm. The wall bushing is mounted on the frame shown in the circle in Fig.3(b). The beams, columns and braces of the steel frame are square tubes with dimensions of 400×400×13 (□400), 300×300×12 (□300) and 150×150×8 (□150), respectively.

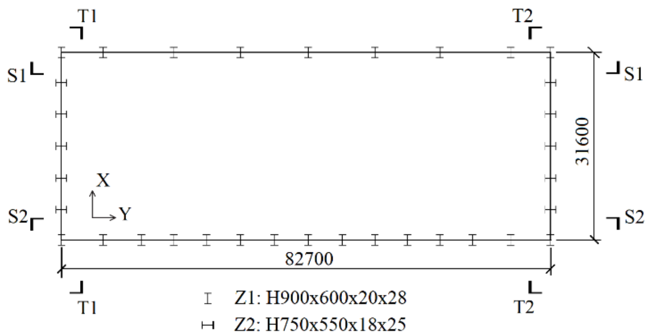

(a) layout view

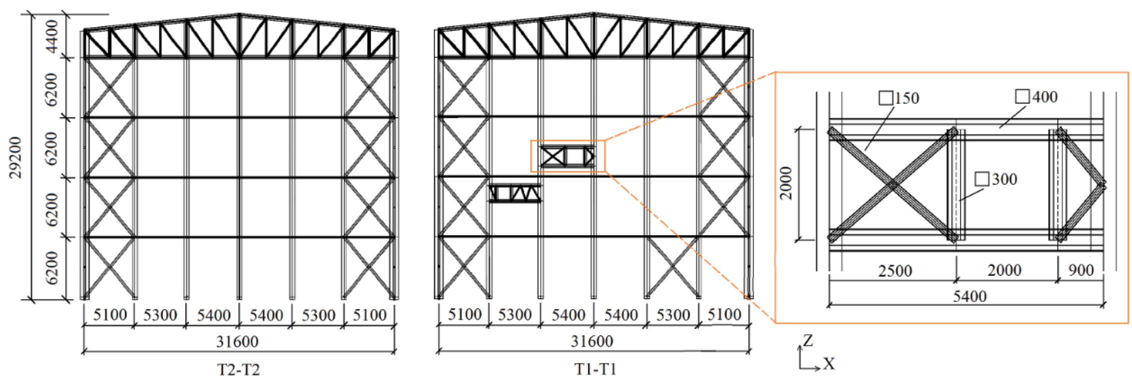

(b) front view (gable wall)

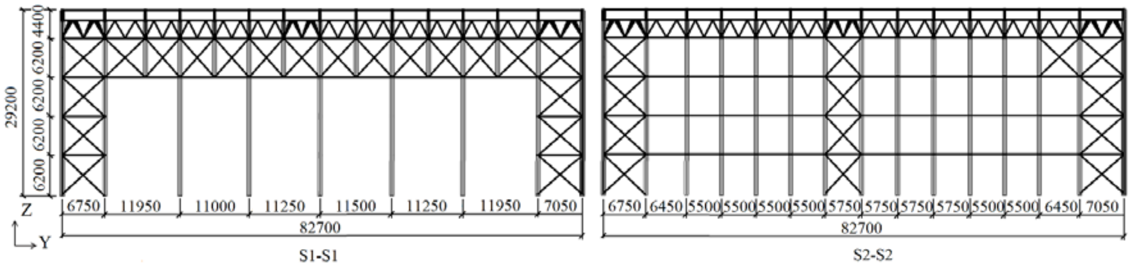

(c) side view

Fig. 3 - Diagram of the ±800 kV UHV valve hall (unit: mm)

2.2 Wall bushing

The UHV bushing is mounted on the gable wall with an angle of 5°and at a height of 14.5 m, and the total length of the bushing is approximately 21 m (Fig.4). The insulators of the wall bushing are made from composite material, which is widely used in electric facilities for insulation and structural functions. The wall bushing contains an indoor bushing, an outdoor bushing and a metal sleeve between the two polymer bushings to install the equipment on the gable wall. An aluminum conductor passing through the wall bushing transmits the electric current from the indoor terminal to the outdoor terminal. A resin-impregnated paper capacitor is wrapped around the conductor to keep the stability of the electromagnetic field and to guarantee the effectiveness of the inner insulation of the wall bushing. Silicon rubber sheds around the external surfaces of the insulators are used for external insulation. The dimensions of the wall bushing mounted on the gable wall of the valve hall are shown in Fig.4 and interior configuration and materials of the wall bushing are shown in Fig.5.

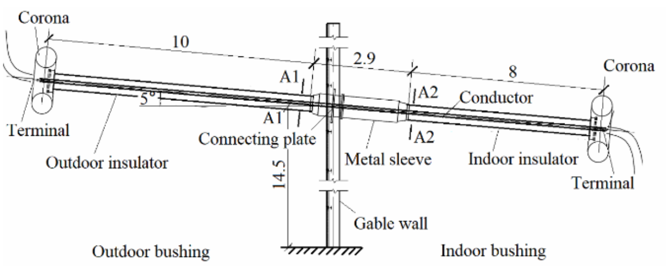

Fig. 4 - Dimensions of the wall bushing (unit: m)

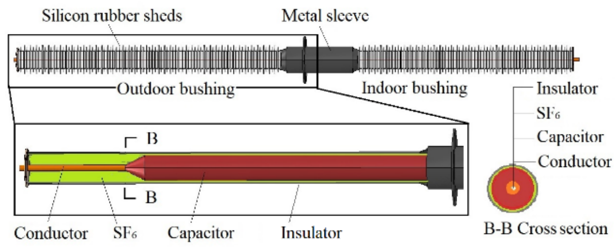

Fig. 5 - Interior configuration and material

2.3 FEM of the whole system and amplification factor of the valve hall

In this analysis, ABAQUS software was employed for the numerical simulations. The beams, columns and braces of the valve hall are simulated by B31 beam elements. Besides, the connecting plate in the valve hall for mounting the bushing is simulated by S4R shell elements. For the wall bushing, the C3D8R solid elements are used to simulate the insulators, conductor and sleeve. Additionally, some simplifications had to be made in the FE model, i.e., a) the silicon rubber sheds outside the insulator for outer insulation were simplified as equivalent masses because Young's modulus of them were small; b) the corona rings were simplified as attached lumped mass; c) the connections of all components in the UHV wall bushing are rigid in the FE model. The FEM and the coordinates of the UHVDC wall bushing-valve hall system is shown in Fig.6. According to the GB 50260 [14] standard and IEEE 693 standard [15], damping ratios of the system were set as 2.0%. To evaluate the seismic vulnerability of the wall bushing-valve hall system by time history analysis, modal frequencies have been first calculated through modal analysis. In mode analysis, the first resonance frequency of the whole system is 1.61 Hz, and the corresponding mode shape is the bending deformation of the wall busing in the X direction. For the valve hall, the first resonance frequency is 2.15 Hz, which was the frequency of the lateral vibration of the structure in the X direction. In addition, the fundamental frequency of the UHV wall bushing mounted on the rigid base (without valve hall) is 2.54 Hz, which indicates that the steel valve hall would decrease the frequencies of the system. To simulate the rigid base, the edge of the bottom plate of the flange of the wall bushing were constrained directly.

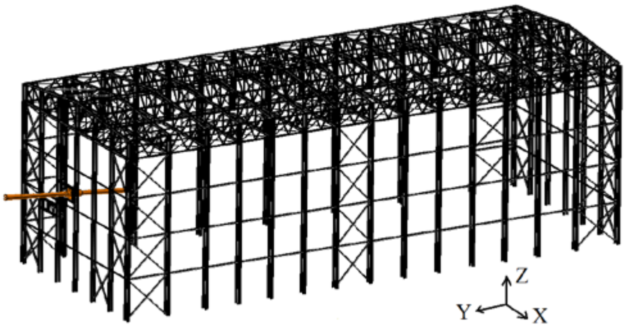

Fig. 6 - FEM and coordinates of the UHVDC wall bushing-valve hall system

To assess the amplification effect of the valve hall and further perform vulnerability analysis on the UHVDC wall bushing, 30 earthquake time histories listed in Table 1 were selected from the Pacific Earthquake Engineering Research Center (PEER) ground motion database based on the site conditions and fortification intensity. The amplification factor of the valve hall is obtained by two means in view of its filtering action, namely time domain method and frequency domain method. Through time domain method, amplification factor is expressed as the ratio of the peak acceleration at the wall bushing's mounting position to that of the input ground motion. While through frequency domain method, amplification factor should be attained by the ratio of the acceleration response spectra value at the wall bushing's installation position to that of the input ground motion at the fundamental frequency of the system (1.61Hz). Results are provided in Fig.7, as shown, the amplification factors are almost below 2.0, which is recommended to be set for the test verification of a ±800 kV UHV wall bushing mounted on a rigid adapter in experiment.

Table 1 - Details of the selected earthquake records

Record No.	Earthquake Name	Year	Station Name	Station No.	Magnitude	V_{s30}(m/s)
RSN11	Northwest Calif-03	1951	Ferndale City Hall	133	5.80	219.31
RSN 12	Kern County	1952	LA - Hollywood Stor FF	326	7.36	316.46
RSN 13	Kern County	1952	Pasadena - CIT Athenaeum	499	7.36	415.13
RSN 14	Kern County	1952	Santa Barbara Courthouse	92	7.36	514.99
RSN 15	Kern County	1952	Taft Lincoln School	148	7.36	385.43
RSN 16	Northern Calif-02	1952	Ferndale City Hall	133	5.20	219.31
RSN 19	Central Calif-01	1954	Hollister City Hall	135	5.30	198.77
RSN 22	El Alamo	1956	El Centro Array #9	75	6.80	213.44
RSN 24	Central Calif-02	1960	Hollister City Hall	135	5.00	198.77
RSN 26	Hollister-01	1961	Hollister City Hall	135	5.60	198.77
RSN 35	Northern Calif-06	1967	Hollister City Hall	135	5.20	198.77
RSN 51	San Fernando	1971	2516 Via Tejon PV	3	6.61	280.56
RSN 53	San Fernando	1971	Bakersfield - Harvey Aud	124	6.61	241.41
RSN 55	San Fernando	1971	Buena Vista - Taft	2	6.61	385.69
RSN 58	San Fernando	1971	Cedar Springs Pumphouse	73	6.61	477.22
RSN 66	San Fernando	1971	Hemet Fire Station	272	6.61	328.09
RSN 67	San Fernando	1971	Isabella Dam (Aux Abut)	137	6.61	591
RSN 69	San Fernando	1971	LB - Terminal Island	81	6.61	217.92
RSN 74	San Fernando	1971	Maricopa Array #1	138	6.61	303.79
RSN 75	San Fernando	1971	Maricopa Array #2	139	6.61	443.85
RSN 76	San Fernando	1971	Maricopa Array #3	140	6.61	441.25
RSN 78	San Fernando	1971	Palmdale Fire Station	82	6.61	452.86
RSN 79	San Fernando	1971	Pasadena - CIT Athenaeum	499	6.61	415.13
RSN 82	San Fernando	1971	Port Hueneme	85	6.61	248.98

RSN 86	San Fernando	1971	San Onofre - So Cal Edison	90	6.61	442.88
RSN 90	San Fernando	1971	UCSB - Fluid Mech Lab	91	6.61	322.42
RSN 96	Managua,	1972	Managua, ESSO	199	5.20	288.77
RSN 399	Coalinga-04	1983	Oil Fields Fire Station - FF	180	5.18	474.15
RSN 1184	Chi-Chi, Taiwan	1999	CHY010	634	7.62	538.69
RSN 1527	Chi-Chi, Taiwan	1999	TCU100	1059	7.62	535.13

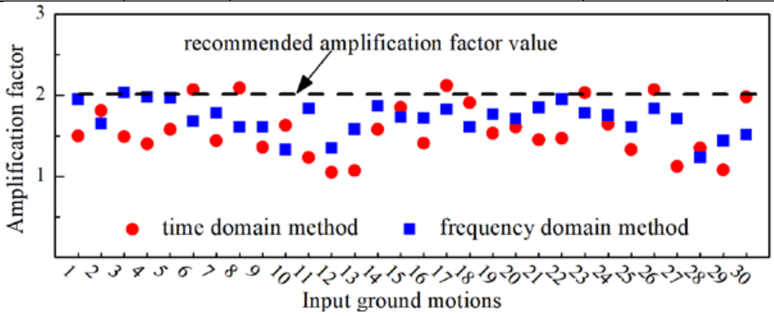

Fig. 7 - Amplification factors of valve hall under different input ground motions

3. Process of developing vulnerability curves

A lognormal cumulative distribution function is often adopted to define a vulnerability function, which is a common assumption that has been confirmed as reasonable in a number of cases[27-30], mathematically expressed as:

$$P(LS|I=x)=\Phi(\frac{\ln x-\mu}{\sigma}) \tag{1}$$

where $P(LS|I=x)$ is the probability that a ground motion with the seismic intensity I = x will cause exceedance of the structural response from the defined limit state; **Φ**( ) denotes the standard normal cumulative distribution function (CDF); μ and σ correspond to the logarithmic median and logarithmic standard deviation of the vulnerability function, respectively. In conventional incremental dynamic analysis (IDA) method, each ground motion in a suite needs to be scaled up until it causes collapse of the structure system, then estimation of $\hat{\mu}$ and $\hat{\sigma}$ can be obtained consistent with the calculating results as:

$$\hat{\mu}=\frac{1}{n}\sum_{i=1}^{n}\ln x_i \tag{2}$$

$$\hat{\sigma}=\sqrt{\frac{1}{n-1}\sum_{i=1}^{n}(\ln x_i-\hat{\mu})^2} \tag{3}$$

where n is the number of ground motions considered and x_i is the seismic intensity value corresponding to the onset of arriving the defined limit state or collapse for the ith ground motion.

However, the traditional IDA method is computationally expensive, as it demands many numerical analyses to be performed with increasing seismic intensity levels in order to finally observe a excess beyond the limit state value. Besides, fragility function values at large-intensity levels are of less interest. Furthermore, it is questionable whether scaling typical moderate-intensity ground motions up to extreme large-intensity levels is an accurate way to represent shaking associated with real occurrences of such large-intensity levels.

3.1 TIDA method

To address these concerns, the TIDA method [26] is put into use, in which each ground motion is only scaled up to some level (x_{max}), above which no further analyses are performed. In this circumstance, If there are generally m ground motions that exceed the defined value of limit state at the seismic intensity levels lower than x_{max}, and n - m ground motions that still do not surpass that value. The maximum likelihood method is applied to compute the likelihood of the data collected.

For the m ground motions that were observed to exceed the defined value of limit state, their seismic intensity values at the onset of exceeding the value of defined limit state for the ith ground motion (x_i) are known. The likelihood that an arbitrary ground motion exceeds the defined value of limit state at x_i, given a fragility function defined by Eq.(1), is the normal distribution probability density function (PDF):

$$\text{Likelihood}=\phi\left(\frac{\ln x_i-\mu}{\sigma}\right) \tag{4}$$

where $\phi()$ denotes the standard normal distribution PDF. And the likelihood that a given ground motion scaled to x_{max} without exceeding the defined value of limit state is the probability that seismic intensity x_i is greater than x_{max}:

$$\text{Likelihood}=1-\Phi\left(\frac{\ln x_{\max}-\mu}{\sigma}\right) \tag{5}$$

Assuming that the x_i value of exceedance for each ground motion is independent, the likelihood of the entire data set collected is the product of the individual likelihoods:

$$\text{Likelihood}=\left[\prod_{i=1}^{m}\phi\left(\frac{\ln x_i-\mu}{\sigma}\right)\right]\left[1-\Phi\left(\frac{\ln x_{\max}-\mu}{\sigma}\right)\right]^{n-m} \tag{6}$$

Using this equation, the fragility function parameters are then obtained by varying the parameters until the likelihood function is maximized. It is mathematically equivalent and numerically easier to maximize the logarithm of this likelihood by the following equation:

$$\{\hat{\mu},\hat{\sigma}\}=\underset{\mu,\sigma}{\arg\max}\sum_{i=1}^{m}\left[\ln\phi\left(\frac{\ln x_i-\mu}{\sigma}\right)\right]+(n-m)\ln\left[1-\Phi(\frac{\ln x_{\max}-\mu}{\sigma})\right] \tag{7}$$

3.2 Introduction damage index

From strength aspect, in past earthquakes, bushings and post insulators have always fractured at their base cross sections (Section A1-A1 and A2-A2 in Fig.4). In this numerical analysis, after inspecting the maximum stress in different parts of the UHV wall bushing model, the most vulnerable location was identified at the bottom of the bushing connecting the wall bushing to the flange of the metal sleeve, which is consistent with the observations in previous earthquakes.

From relative deformation aspect inside the UHV wall bushing, under the action of an earthquake, a relatively large deformation and even collision will occur between the internal conductive rod (wrapped with insulating body-capacitor) of the wall bushing and the outer insulator sleeve (Section B-B in Fig.5). This phenomenon has never been noticed before, which may affect the insulation performance and electrical function of the UHV wall bushing. In this numerical analysis, after inspecting the maximum relative deformation along the overall length of the UHV wall bushing model, the most vulnerable location was identified at the end section of the insulating body.

Therefore, the stress responses at the base cross sections of the indoor and outdoor insulators, and the relative deformation between inner conductor and outer insulator at the end section of the insulating capacitor body are critical indicators for evaluating the seismic performance of the UHV wall bushing, as exhibited in Fig.8.

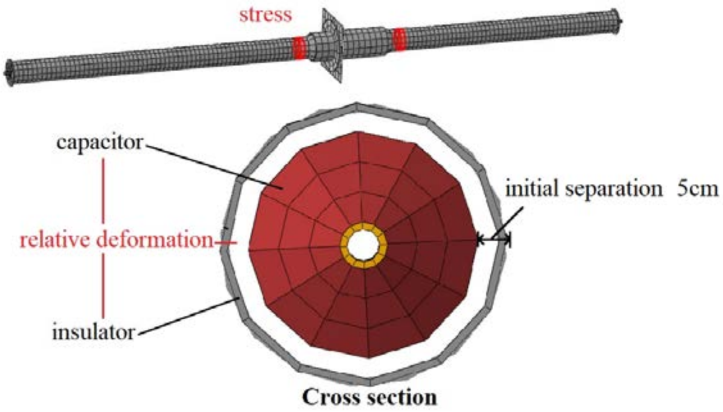

Fig. 8 - Seismic vulnerable locations

Strength failure has been defined in the different versions of IEEE standard. According to the latest version, the maximum allowable stress in a porcelain section is as much as 50% of the ultimate strength of the material. In the 1985 version of IEEE standard, the allowable stress varies from 25% to 50%. In this study, two damage limit states have been considered, one for moderate damage (equal to 25% of the ultimate strength), and the other for severe damage (equal to 50% of the ultimate strength). Considering the ultimate strength of 75 MPa for the insulator material provided by the manufacturer, the corresponding maximum allowable stress for moderate and severe damage limit states are 18.75 MPa and 37.5 MPa, respectively.

However, scant attention has been paid to the relative deformation failure problem and the explicit specification in the relevant current standards is still vacant. In this analysis, for the sake of unification and classification, two damage limit states have been considered, one for moderate damage (equal to 50% of the ultimate relative deformation), and the other for severe damage (equal to 100% of the ultimate relative deformation). Considering the ultimate relative deformation of 5 cm confined by the initial fixed separation between the outer insulator and inner capacitor, the corresponding maximum allowable relative deformation for moderate and severe damage limit states are 2.5 cm and 5 cm, respectively.

3.3 Vulnerability curves and discussion

According to the calculating records obtained from time history analysis (THA) and based on the description of TIDA method, parameters of fragility fonction ($\hat{\mu}$ and $\hat{\sigma}$) for moderate and severe damage limit states from strength and deformation aspects have been estimated and listed in Table 2. Accordingly, vulnerability curves for the two predefined damage limit states considering strength and relative deformation aspects are presented in Fig.9 and Fig.10, respectively. As shown, the estimated vulnerability curves and the corresponding sample points agree very well, confirming the assumption that the vulnerability curve of the wall bushing satisfies the law of lognormal cumulative distribution function and proving the validity of this TIDA method to develop a vulnerability curve.

Table 2 - Fragility parameters for different damage limit states from strength and deformation aspects

Parameters Estimation	Strength aspect				Deformation aspect			
	Indoor bushing		Outdoor bushing		Indoor bushing		Outdoor bushing	
	moderate	severe	moderate	severe	moderate	severe	moderate	severe
$\hat{\mu}$	-1.559	-0.619	-2.144	-1.067	-0.761	-0.130	-1.228	-0.444
$\hat{\sigma}$	0.300	0.300	0.341	0.341	0.349	0.384	0.307	0.307

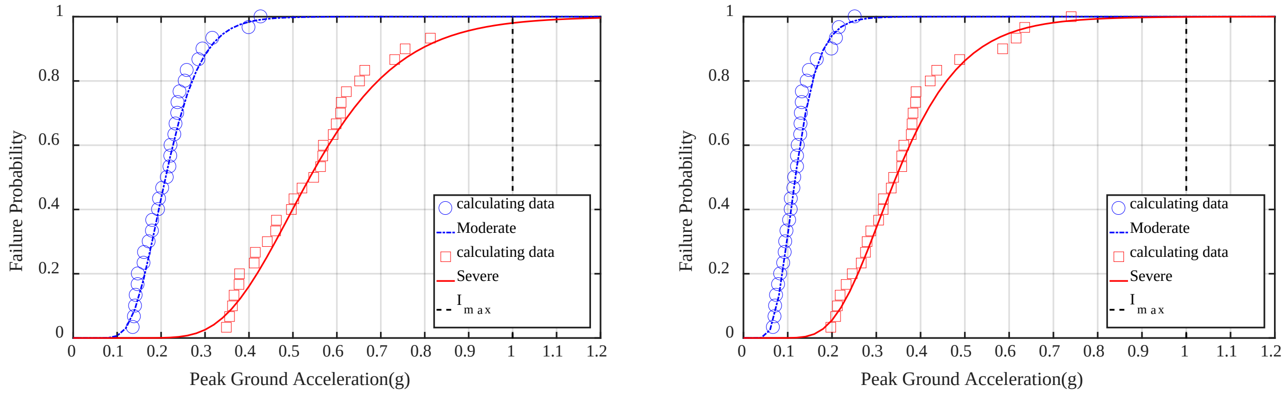

(a) Indoor bushing (b) Outdoor bushing

Fig. 9 - Vulnerability curves for different levels of damage limit states from strength aspect

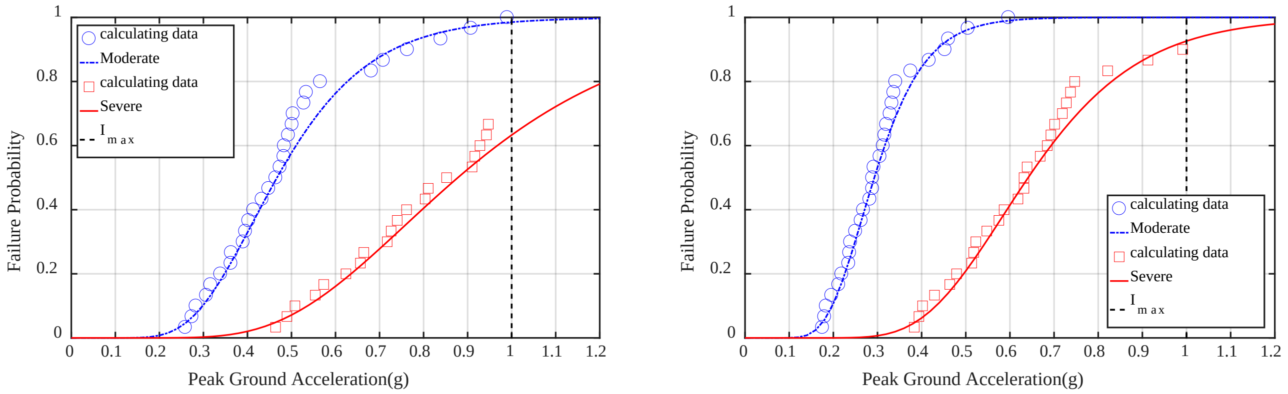

(a) Indoor bushing (b) Outdoor bushing

Fig. 10 - Vulnerability curves for different levels of damage limit states from deformation aspect

In view of the ultimate strength of the insulator material and the maximum stress at the base cross sections of wall bushing in Fig.9, the failure probability of moderate damage limit state for the indoor and outdoor bushings with the peak ground acceleration (PGA) = 0.2 g would be 44% and 95% respectively, which indicates that the failure probability of moderate damage limit state is noticeable for the indoor bushing and almost inevitable for the outdoor bushing, even under ground motions with low PGA amplitudes. Besides, both indoor and ourdoor bushings wouldn't encounter severe damage until PGA larger than 0.2 g, and it might be acceptable for indoor bushing to suffer ground motions with PGA lower than 0.4 g as its failure probability of severe damage keeps quite low. While it would be very likely for the outdoor bushing to experience severe damage under the earthquake with the fortification intensity of 0.4 g, for the corresponding failure probability is near to 70%. The outdoor bushing is much more seismic vulnerable compared with the indoor bushing owing to its longer length, heavier weight and lower stiffness.

Similarly, the same conclusion can be drawn from the comparison between indoor and outdoor bushings considering the relative deformation aspect in Fig.10. It should be noted that to what extent will the relative displacement between internal capacitor and outer insulator affect the insulation performance, and electromagnetic stability inside the wall bushing still remains unknown at present. And hence the damage index and the definition of limit states for the relative deformation in this vulnerability analysis may be somewhat inaccurate, for instance, if the relative deformation damage index for the severe damage changes from the predefined 100% to 50% of the ultimate relative deformation, the original vulnerability curves of moderate damage may accordingly represent the severe damage limit state under the new definition of relative deformation damage index, as illustrated in Fig.11. In this circumstance, the failure probability caused by excessive relative deformation is even higher than that caused by insufficient material strength, which suggests that the wall bushing would be out of service even if the structure is intact under earthquakes. Therefore, much more attention should be paid to the influence on electromagnetic stability of the wall bushing caused by excessive relative deformation inside. And the damage limit states and corresponding thresholds should be investigated and determined under the cooperation with experts in the field of electronics and electrical insulation before conducting the vulnerability analysis and evaluating the seismic performance form deformation aspect.

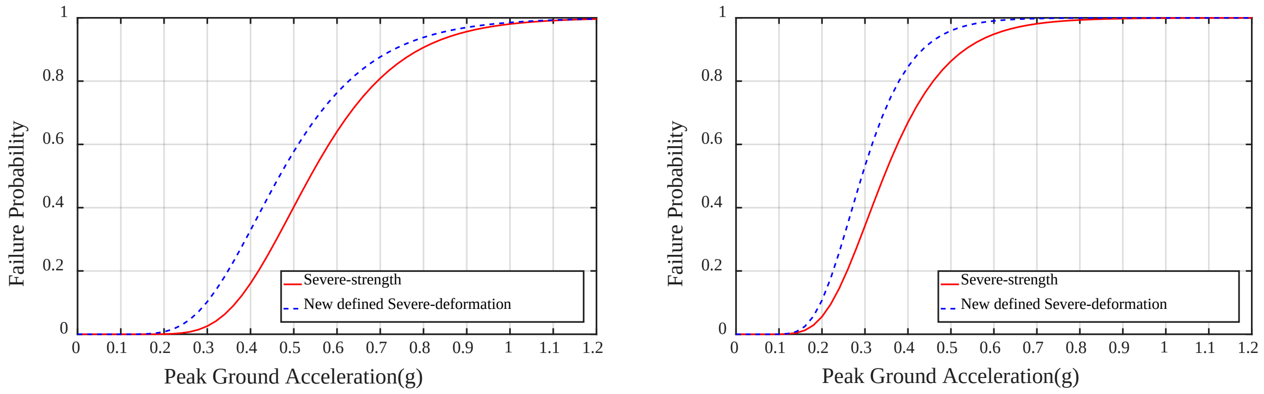

(a) Indoor bushing (b) Outdoor bushing

Fig. 11 - Vulnerability curves for severe damage from strength and deformation aspect

4. Conclusion

Considering the critical role of substations and converter stations in electric supply during and after earthquakes, the seismic performance of the wall bushing, one of the key elements in converter substations, was evaluated. A FEM of ±800kV UHVDC wall bushing-valve hall system was established, and its analytical seismic vulnerability curves for two damage states of moderate and severe from strength and deformation aspects were developed after a number of THA. The TIDA method was adopted for estimating vulnerability curves. Based on the conducted numerical analyses it can be concluded that:

The valve hall structure would decrease the as-mounted frequencies of the wall bushing and amplify the seismic loading to the wall bushing with a maximum amplification factor of 2.0, which cannot be neglected when evaluating the seismic performance of wall bushing.

The base cross section of the outdoor bushing has the highest seismic vulnerability and would be very likely to experience severe damage under the earthquake with the fortification intensity (0.4 g).

More attentions should be paid to the influence on electromagnetic stability and insulation performance of the wall bushing caused by excessive relative deformation inside, and the damage limit states and corresponding thresholds need to be determined cooperated with experts in electric engineering.

5. Acknowledgements

This study was financially supported by the National Natural Science Foundation of China (Grant No. 51878508). The support is greatly appreciated.

6. References

References must be cited in the text in square brackets [1, 2], numbered according to the order in which they appear in the text, and listed at the end of the manuscript in a section called References, in the following format:

[1] A.J. Schiff (1998): Guide to improved earthquake performance of electric power systems. US Department of Commerce, National Institute of Standards and Technology.

[2] A.J. Schiff (1995): Northridge earthquake: lifeline performance and post-earthquake response. ASCE.

[3] Q. Xie, R. Zhu (2011): Damage to electric power grid infrastructure caused by natural disasters in China. *IEEE Power and Energy Magazine*. **9**(2), 28-36

[4] A. Kwasinski A, J. Eidinger J, A. Tang A (2014): Performance of electric power systems in the 2010-2011 Christchurch, New Zealand, earthquake sequence. *Earthquake Spectra*, **30**(1), 205-230.

[5] D. Huang, Y. Shu, J. Ruan, Y. Hu (2009): Ultra high voltage transmission in China: developments, current status and future prospects. *Proceeding of the IEEE*, **97**(3), 555-583.

[6] Y. Shu, W. Chen (2018): Research and application of UHV power transmission in China. *High Voltage*, 3(1), 1-13.(in Chinese)

[7] A.S. Whittaker, G.L. Fenves, A.S.J. Gilani (2007): Seismic evaluation and analysis of highvoltage substation disconnect switches, *Engineering Structure*, **29**(12), 3538–3549.

[8] C. He, Q. Xie, Z. Yang (2019): Seismic evaluation and analysis of 1100-kVUHV porcelain transformer bushings. *Soil Dynamics And Earthquake Engineering*, **123**(8), 498-512.

[9] R.K. Mohammadi, V. Akrami, F. Nikfar (2012): Dynamic properties of substation support structures. *Journal of Constructional Steel Research*, **78**(6), 173-182.

[10] M. Koliou, A. Filiatrault, A.M. Reinhorn (2013): Seismic response of high-voltage transformer-bushing systems incorporating flexural stiffeners II: experimental study. *Earthquake Spectra*, **29**(4), 1353-1367.

[11] R. Villaverde, G.C. Pardoen, S. Carnalla (2001): Ground motion amplification at flange level of bushings mounted on electric substation transformers. *Earthquake Engineering and Structural Dynamics*, (30), 621-632.

[12] A. Filiatrault, H. Matt (2005): Experimental seismic response of high voltage transformer-bushing systems. *Earthquake Spectra*, **21**(4), 1009-1025.

[13] M. Koliou, A. Filiatrault, A.M. Reinhorn (2013): Seismic response of high-voltage transformer-bushing systems incorporating flexural stiffeners I: Numerical study. *Earthquake Spectra*, **29**(4), 1335–1352.

[14] GB 50260 (2013): *Code for Seismic Design of Electrical Installations*, Beijing, (in Chinese).

[15] IEEE Standard 693 (2017): *IEEE Recommended Practice for Seismic Design of Substations*, New York,.

[16] C. Camensig, L. Breseti, S. Clementel, M. Salvetti (1997): Seismic risk evaluation for high voltage air insulated substation. *Journal of Reliability Engineering and System Safety*, **55**, 179–91.

[17] Sh. Takada, M. Bastami, Y. Kuwata, M.B. Javanbarg (2004): Performance of electric power systems during the Bam earthquake and its fragility analyses. Kobe University, Japan: *Memoirs of Construction Engineering Research Institute*, **46**, 141–52.

[18] M.A. Jaigirdar (2005): Seismic Fragility and risk analysis of electric power substations. Master of Engineering thesis. Montreal, Quebec: *Department of Civil Engineering and Applied mechanics*, McGill University;.

[19] F. Paolacci, R. Giannini, S. Alessandri (2014): Seismic vulnerability assessment of a high voltage disconnect switch. *Soil Dynamics And Earthquake Engineering*, **67**, 198–207.

[20] S.A. Zareei, M. Hosseini, M. Ghafory-Ashtiany (2016): Seismic failure probability of a 400kV power transformer using analytical fragility curves. *Engineering Failure Analysis*, **70**, 273-289.

[21] S.A. Zareei, M. Hosseini, M. Ghafory-Ashtiany (2017): Evaluation of power substation equipment seismic vulnerability by multivariate fragility analysis:A case study on a 420 kV circuit breaker. *Soil Dynamics and Earthquake Engineering*, (92), 79-94.

[22] F. Paolacci, R. Giannini (2009): Seismic reliability assessment of a high-voltage disconnect switch using an effective fragility analysis. *Journal of Earthquake Engineering*, **13**(2), 217-235.

[23] D. Straub, A.D. Kiureghian (2008): Improved seismic fragility modeling from empirical data. *Structural Safety*, **30**(4), 320-336.

[24] D. Vamvatsikos, C.A. Cornell (2002): Incremental dynamic analysis. *Earthquake Engineering & Structural Dynamics*, 31, 491–514.

[25] D. Vamvatsikos, C.A. Cornell (2004): Applied incremental dynamic analysis. *Earthquake Spectra*, 20, 523–553.

[26] J.W. Baker (2015): Efficient analytical fragility function fitting using dynamic structural analysis. *Earthquake Spectra*, **31**(1), 579–599.

[27] K. Porter, R. Kennedy, R. Bachman (2007): Creating fragility functions for performancebased earthquake engineering. *Earthquake Spectra*, 23, 471–489.

[28] B.A. Bradley, R.P. Dhakal (2008): Error estimation of closed-form solution for annual rate of structural collapse. *Earthquake Engineering & Structural Dynamics*, 37, 1721–1737.

[29] M. Ghafory-Ashtiany, M. Mousavi, A. Azarbakht (2011): Strong ground motion record selection for the reliable prediction of the mean seismic collapse capacity of a structure group. *Earthquake Engineering & Structural Dynamics*, 40, 91–708.

[30] L. Eads, E. Miranda, H. Krawinkler (2013): An efficient method for estimating the collapse risk of structures in seismic regions. *Earthquake Engineering & Structural Dynamics*, 42, 25–41.

